Pergamon

PII: S0042-6989(96)00178-2

Vision Res., Vol. 36, No. 24, pp. 4059–4068, 1996

Printed in Great Britain
0042-6989/96 $15.00 + 0.00

Ionic Current Model of the Vertebrate Rod Photoreceptor

Y. KAMIYAMA,* T. OGURA,* S. USUI*†

We describe voltage- and calcium-dependent ionic currents in the photoreceptor inner segments similar to the Hodgkin and Huxley (*Journal of Physiology*, *117*, 500–544, 1952) equations. The model is used to describe both rods and cones by adjusting parameters. To simulate the light response, the inner segment model was connected with the phototransduction model proposed by Torre *et al.* (*Cold Spring Harbor Symposia on Quantitative Biology*, *55*, 563–573, 1990). The role of individual ionic currents in the inner segment in shaping the light response was analyzed through computer simulations. The results suggest that: (1) the transient hyperpolarization to a bright flash is generated by I_h; (2) the oscillation after prolonged hyperpolarization in rods results from the interaction among I_{Ca}, $I_{K(Ca)}$, and $I_{Cl(Ca)}$. Since the present model describes the biophysical processes from phototransduction to voltage response, the model can be used for analyzing the light response properties of the photoreceptors quantitatively. Copyright © 1996 Elsevier Science Ltd.

Photoreceptor Ionic current model Simulation analysis

INTRODUCTION

Vertebrate photoreceptors respond to light with graded membrane hyperpolarization. It is widely accepted that the cGMP-activated conductance of the outer segment generates the electrical response to light in the vertebrate photoreceptors [reviewed in Yau & Baylor (1989); McNaughton (1990)]. However, the response is not only determined by the light-sensitive conductivity change in the outer segment, but is also affected by voltage-dependent conductances located in the inner segment (Attwell & Wilson, 1980; Bader *et al.*, 1982; Baylor *et al.*, 1984; Maricq & Korenbrot, 1988, 1990a, b; Barnes & Hille, 1989), which play a significant role in shaping the electrical signal of vertebrate photoreceptors.

The purpose of this paper is to clarify how the photoreceptor encodes the light signal into the electrical signal. The strategy is to develop a model of the photoreceptor based on a variety of experimental results already published. A similar model has been constructed for retinal horizontal cells (Usui *et al.*, 1996a). This approach is essential for clarifying the role of individual ionic current and the relationship between the photocurrent and the photovoltage response. First, we constructed a quantitative model of the inner segment based on the voltage clamp studies by Bader *et al.* (1982), Maricq and Korenbrot (1988, 1990a, b) and Barnes and Hille (1989). Secondly, the model of the inner segment was connected with the phototransduction model proposed by Torre *et al.* (1990). Finally, by using the complete model of the photoreceptor, we simulated the light response of the rod photoreceptors and analyzed the electrical properties quantitatively.

SUMMARY OF IONIC CURRENTS IN PHOTORECEPTORS' INNER SEGMENTS

We first briefly review the ionic currents identified in photoreceptor inner segments. There are at least three voltage-dependent ionic currents and two calcium-dependent ionic currents in the inner segments, namely, hyperpolarization activated current (I_h), delayed rectifying potassium current (I_{Kv}), calcium current (I_{Ca}), Ca-dependent potassium current [$I_{K(Ca)}$], and Ca-dependent chloride current [$I_{Cl(Ca)}$], which are summarized in Table 1. These currents are observed in a variety of rods, salamander cones and lizard cones. Figure 1 shows an electrical equivalent circuit of a photoreceptor which includes the photocurrent in the outer segment and ionic currents in the inner segment. Since both rod and cone inner segments have similar ionic currents (Bader *et al.*, 1982; Barnes & Hille, 1989), we made no distinction between rods and cones when referring to the ionic currents, except for a special case described in each section.

*Biological and Physiological Engineering Laboratory, Department of Information and Computer Sciences, Toyohashi University of Technology, Toyohashi 441, Japan.

†To whom all correspondence should be addressed [*Email* usui@bpel.tutics.tut.ac.jp].

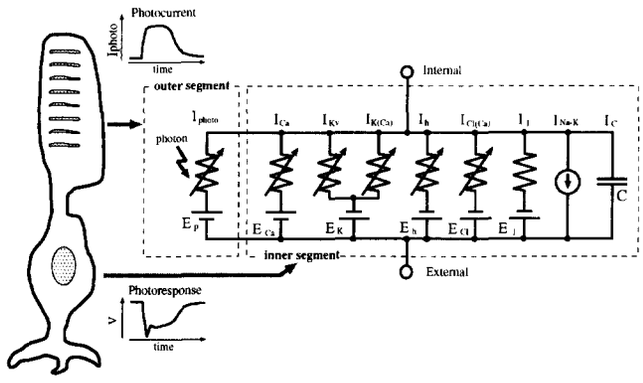

FIGURE 1. An electrical equivalent circuit model of a photoreceptor.

DESCRIPTION OF IONIC CURENTS IN THE INNER SEGMENT

The membrane model for the photoreceptor model produces the following ordinary differential equation:

$$C\frac{dV}{dt} = -(I_{photo} + I_{Kv} + I_h + I_{Ca} + I_{K(Ca)} + I_{Cl(Ca)} + I_l + I_{Na-K}). \quad (1)$$

We expressed these ionic currents using a mathematical formulation similar to the Hodgkin–Huxley equations (Hodgkin & Huxley, 1952). In general, each current is described by an equation of the form

$$I_{ion}(V,t) = \overline{g_{ion}} \cdot m^M(V,t) \cdot h(V,t) \cdot (V - E_{ion}) \quad (2)$$

where $\overline{g_{ion}}$ is the maximum conductance, m is the activation variable, h is the inactivation variable, M is the gating exponent and E_{ion} is the reversal potential. Each ionic current was modeled independently from the pharmacologically isolated characteristics. We also introduced an intracellular calcium concentration system, needed to model the calcium-dependent currents. Full descriptions of the proposed model are given in Tables 2 and 3; the data used to derive the exact model and fit parameters for each ionic current component are explained in the following subsections.

Delayed rectifying potassium current, I_{Kv}

Experimental evidence (Bader *et al.*, 1982; Maricq & Korenbrot, 1990b) shows that the inner segment of the photoreceptor contains a voltage-dependent potassium current which is blocked by tetraethylammonium (TEA) and has characteristics typical of a delayed rectifier. Although Maricq and Korenbrot (1990b) suggest that there exist at least two subtypes of delayed rectifying potassium currents within the same cell, most experimental data can be fitted by a single delayed rectifying potassium current model, and thus we did not distinguish between the subtypes. We estimated the model parameters from the voltage clamp measurements by Maricq and Korenbrot (1990b) in the presence of Co^{2+} and Cs^+.

Hyperpolarization-activated current, I_h

I_h is a slowly developing inward current activated by membrane hyperpolarization (Barnes & Hillo, 1989; Wollmuth & Hille, 1992). Barnes and Hille (1989) proposed a simple kinetic model of this current. The gating kinetics of I_h is described by a five-state model with two closed and three open states, governed by voltage-dependent rate constants as shown in Table 2. We used their formulation and estimated the parameters from the measurement by Maricq and Korenbrot (1990a).

Calcium current, I_{Ca}

I_{Ca} is activated by depolarization from about −40 mV; the maximum current is observed at a voltage of about 0 mV; the current decreases at more depolarization; and the reversal potential is more positive than +50 mV (Maricq & Korenbrot, 1988). The current is activated within a few milliseconds and shows little inactivation, and thus we omitted the dynamics of the inactivation process as shown in Table 2. The model parameters were estimated from the experimental data by Maricq and Korenbrot (1988). Since cytosolic calcium ions have a spatial distribution, the value of the reversal potential for calcium is determined by the Nernst equation using the calcium concentration just below the membrane ($[Ca^{2+}]_s$) and the extracellular concentration ($[Ca^{2+}]_o$).

Calcium-dependent chloride current, $I_{Cl(Ca)}$

$I_{Cl(Ca)}$ is activated by depolarization above −40 mV, and the rate of activation and inactivation is closely related to the intracellular concentration of free Ca^{2+}. We therefore expressed the activation variable (m_{Cl}) as a sigmoidal function of the free Ca^{2+} ($[Ca^{2+}]_s$) as shown in Table 2.

Calcium-dependent potassium current, $I_{K(Ca)}$

$I_{K(Ca)}$ is activated by membrane depolarization; the maximum magnitude of the current is at about +20 mV; and the current decreases with increased depolarization (Barnes & Hille, 1989). The magnitude of this current is varied depending on cell to cell and/or species (Barnes &

TABLE 1. Summary of ionic currents identified in photoreceptor inner segment

Ionic currents	Permeant ions	Reversal potential [mV]	Blockers	Activation
I_h	Na^+, K^+	−32	Cs	< −30 mV
I_{Kv}	K^+	−80	TEA	> −70 mV
I_{Ca}	Ca^{2+}	100 ~ 130	Co	> −45 mV
$I_{K(Ca)}$	K^+	−80	Co, BAPTA, EGTA	Calcium entry, > −30 mV
$I_{Cl(Ca)}$	Cl^-	−55 ~ −40	Co, BAPTA, EGTA, NFA	Calcium entry, > −40 mV

TABLE 2. A mathematical formulation of each ionic current of a photoreceptor

Delayed rectifying K *current*

$$\alpha_{m\mathrm{K}} = \frac{5(100 - V)}{\exp\left(\frac{100-V}{42}\right) - 1}$$

$$\beta_{m\mathrm{K}} = 9\exp\left(-\frac{V - 20}{40}\right)$$

$$\frac{\mathrm{d}m_{\mathrm{K}}}{\mathrm{d}t} = \alpha_{m\mathrm{K}} \cdot (1 - m_{\mathrm{K}}) - \beta m_{\mathrm{K}} \cdot m_{\mathrm{K}}$$

$$\alpha_{h\mathrm{K}} = 0.15\exp\left(-\frac{V}{22}\right)$$

$$\beta_{\mathrm{hK}} = \frac{0.4125}{\exp\left(\frac{10-V}{7}\right) + 1}$$

$$\frac{\mathrm{d}h_{\mathrm{K}}}{\mathrm{d}}t = \alpha_{h\mathrm{K}} \cdot (1 - h_{\mathrm{K}}) - \beta_{h\mathrm{K}} \cdot h_{\mathrm{K}}$$

$$I_{\mathrm{Kv}} = \overline{g_{\mathrm{Kv}}} \cdot (m_{\mathrm{K}})^3 \cdot h_{\mathrm{K}} \cdot (V - E_{\mathrm{K}})$$

$$\overline{g_{\mathrm{Kv}}} = 2.0\ [\mathrm{nS}]$$

$$E_{\mathrm{K}} = -80\ [\mathrm{mV}]$$

Ca *current*

$$\alpha_{\mathrm{Ca}} = \frac{300(80 - V)}{\exp\left(\frac{80-V}{25}\right) - 1}$$

$$\beta_{\mathrm{Ca}} = \frac{1000}{1 + \exp\left(\frac{V+38}{7}\right)}$$

$$\frac{\mathrm{d}m_{\mathrm{Ca}}}{\mathrm{d}t} = \alpha_{\mathrm{Ca}} \cdot (1 - m_{\mathrm{Ca}}) - \beta_{\mathrm{Ca}} \cdot m_{\mathrm{Ca}}$$

$$E_{\mathrm{Ca}} = 12.9\log\left(\frac{[\mathrm{Ca}^{2+}]_{\mathrm{o}}}{[\mathrm{Ca}^{2+}]_{\mathrm{s}}}\right)$$

$$m_{\mathrm{Ca\,h}} = \frac{\exp\left(\frac{40-V}{18}\right)}{1 + \exp\left(\frac{40-V}{18}\right)}$$

$$I_{\mathrm{Ca}} = \overline{g_{\mathrm{Ca}}} \cdot (m_{\mathrm{Ca}})^4 \cdot m_{\mathrm{Ca\,h}} \cdot (V - E_{\mathrm{Ca}})$$

$$\overline{g_{\mathrm{Ca}}} = 1.2\ [\mathrm{nS}]$$

Ca-*dependent* Cl *current*

$$m_{\mathrm{Cl}} = \frac{1}{1 + \exp\left(\frac{\mathrm{Cl_h} - [\mathrm{Ca}^{2+}]_{\mathrm{s}}}{0.09}\right)}$$

$$I_{\mathrm{Cl(Ca)}} = \overline{g_{\mathrm{Cl}}} \cdot m_{\mathrm{Cl}} \cdot (V - E_{\mathrm{Cl}})$$

$$\overline{g_{\mathrm{Cl}}} = 6.5\ [\mathrm{nS}]$$

$$E_{\mathrm{Cl}} = -45\ [\mathrm{mV}]$$

$$Cl_{\mathrm{h}} = 0.37\ [\mu\mathrm{M}]$$

Ca-*dependent* K *current*

$$\alpha_{\mathrm{Kc}} = \frac{15(80 - V)}{\exp\left(\frac{80-V}{40}\right) - 1}$$

$$\beta_{\mathrm{Kc}} = 20\exp\left(-\frac{V}{35}\right)$$

$$\frac{\mathrm{d}m_{\mathrm{Kc}}}{\mathrm{d}t} = \alpha_{\mathrm{Kc}}(1 - m_{\mathrm{Kc}}) - \beta_{\mathrm{Kc}} \cdot m_{\mathrm{Kc}}$$

$$m_{\mathrm{Kc1}} = \frac{[\mathrm{Ca}^{2+}]_{\mathrm{s}}}{[\mathrm{Ca}^{2+}]_{\mathrm{s}} + 0.3}$$

$$I_{\mathrm{K(Ca)}} = \overline{g_{\mathrm{Kc}}} \cdot (m_{\mathrm{Kc}})^2 \cdot m_{\mathrm{Kc1}} \cdot (V - E_{\mathrm{K}})$$

$$\overline{g_{\mathrm{Kc}}} = 0.5\ [\mathrm{nS}]$$

Leakage current

$$I_{\mathrm{L}} = gl \cdot (V - E_{\mathrm{l}})$$

$$gl = 0.5\ [\mathrm{nS}]$$

$$E_{\mathrm{l}} = -55\ [\mathrm{mV}]$$

Na–K *exchanger current*

$$I_{\mathrm{Na\text{-}K}} = 9.6\ [\mathrm{pA}]$$

Capacitance

$$C = 10\ [\mathrm{pF}]$$

Hyperpolarization activated current

$$\alpha_{\mathrm{h}} = \frac{3}{\exp\left(\frac{V+88}{14}\right) + 1}$$

$$\beta_{\mathrm{h}} = \frac{20}{\exp\left(-\frac{V+18}{20}\right) + 1}$$

$$\mathrm{M} = [C_1\ C_2\ O_1\ O_2\ O_3]^t$$

$$\frac{\mathrm{d}}{\mathrm{d}t}\mathrm{M} = \mathrm{KM}$$

$$m_{\mathrm{h}} = O_1 + O_2 + O_3$$

$$I_{\mathrm{h}} = \overline{g_{\mathrm{h}}} \cdot m_{\mathrm{h}} \cdot (V - E_{\mathrm{h}})$$

$$\overline{g_{\mathrm{h}}} = 0.305\ [\mathrm{nS}]$$

$$E_{\mathrm{h}} = -32\ [\mathrm{mV}]$$

$$K = \begin{bmatrix} -4\alpha_{\mathrm{h}} & \beta_{\mathrm{h}} & 0 & 0 & 0 \\ 4\alpha_{\mathrm{h}} & -(\beta_{\mathrm{h}} + 3\alpha_{\mathrm{h}}) & 2\beta_{\mathrm{h}} & 0 & 0 \\ 0 & 3\alpha_{\mathrm{h}} & -(2\beta_{\mathrm{h}} + 2\alpha_{\mathrm{h}}) & 3\beta_{\mathrm{h}} & 0 \\ 0 & 0 & 3\alpha_{\mathrm{h}} & -(3\beta_{\mathrm{h}} + \alpha_{\mathrm{h}}) & 4\beta_{\mathrm{h}} \\ 0 & 0 & 0 & \alpha_{\mathrm{h}} & -4\beta_{\mathrm{h}} \end{bmatrix}$$

TABLE 3. Model of intracellular calcium mechanism

$$\frac{d}{dt}[Ca^{2+}]_s = \frac{I_{Ca}}{2FV_1} - \frac{I_{ex}+I_{ex2}}{2FV_1} - D_{Ca}\frac{S_1}{V_1\delta}([Ca^{2+}]_s - [Ca^{2+}]_f)$$
$$+Lb_2[Ca^{2+}]_{ls} - Lb_1[Ca^{2+}]_s(BL - [Ca^{2+}]_{ls}) - Hb_1[Ca^{2+}]_s(BH - [Ca^{2+}]_{hs})$$
$$+Hb_2[Ca^{2+}]_{hs}$$

$$\frac{d}{dt}[Ca^{2+}]_f = D_{Ca}\frac{S_1}{V_2\delta}([Ca^{2+}]_s - [Ca^{2+}]_f) + Lb_2[Ca^{2+}]_{lf} - Lb_1[Ca^{2+}]_f(BL - [Ca^{2+}]_{lf})$$
$$-Hb_1[Ca^{2+}]_f(BH - [Ca^{2+}]_{hf}) + Hb_2[Ca^{2+}]_{hf}$$

$$\frac{d}{dt}[Ca^{2+}]_{ls} = Lb_1[Ca^{2+}]_s(BL - [Ca^{2+}]_{ls}) - Lb_2[Ca^{2+}]_{ls}$$

$$\frac{d}{dt}[Ca^{2+}]_{hs} = Hb_1[Ca^{2+}]_s(BH - [Ca^{2+}]_{hs}) - Hb_2[Ca^{2+}]_{hs}$$

$$\frac{d}{dt}[Ca^{2+}]_{lf} = Lb_1[Ca^{2+}]_f(BL - [Ca^{2+}]_{lf}) - Lb_2[Ca^{2+}]_{lf}$$

$$\frac{d}{dt}[Ca^{2+}]_{hf} = Hb_1[Ca^{2+}]_f(BH - [Ca^{2+}]_{hf}) - Lb_2[Ca^{2+}]_{hf}$$

$$I_{ex} = I_{max}\cdot\exp(-\frac{V+14}{70})\cdot\frac{([Ca^{2+}]_s - Ca_e)}{([Ca^{2+}]_s - Ca_e)+2.3}$$

$$I_{ex2} = I_{max2}\cdot\frac{([Ca^{2+}]_s - Ca_e)}{([Ca^{2+}]_s - Ca_e)+0.5}$$

V, Membrane potential [mV]; I_{Ca}, calcium current [pA]; I_{ex}, $Na^+ - Ca^{2+}$ exchanger current [pA]; I_{ex2}, Ca–ATPase pump current [pA]; F, Faraday constant; $[Ca^{2+}]_s$, Ca concentration in submembrane area; $[Ca^{2+}]_f$, Ca concentration in free intracellular area; $[Ca^{2+}]_{hs}$, submembrane Ca concentration bound to high affinity buffer; $[Ca^{2+}]_{ls}$, submembrane Ca concentration bound to low affinity buffer; Ca_e, minimum intracellular Ca concentration, 0.05 [μM]; $[Ca^{2+}]_{hf}$, free intracellular Ca concentration bound to high affinity buffer; $[Ca^{2+}]_{lf}$, free intracellular Ca concentration bound to low affinity buffer; BH, maximum concentration of high-affinity buffer, 500 [μM]; BL, maximum concentration of low-affinity buffer, 300 [μM]; Lb_1, Lb_2, on and off rate constants for the binding of Ca to low affinity buffer, 0.4 [$sec^{-1}\ \mu M^{-1}$], 0.2 [sec^{-1}]; Hb_1, Hb_2, on and off rate constants for the binding of Ca to high affinity buffer, 100 [$sec^{-1}\ \mu M^{-1}$], 90 [sec^{-1}]; V_1, volume of submembrane area 3.664×10^{-12} [l]; V_2, volume of deep intracellular area 5.236×10^{-13} [l]; S_1, submembrane area 3.14×10^{-6}; D_{Ca}, diffusion coefficient for Ca; δ, diffusion distance, 3×10^{-4} [cm]; I_{max}, maximum $Na^+ - Ca^{2+}$ exchanger current 20 [pA]; I_{max2}, maximum Ca-ATPase pump current 30 [pA].

Hille, 1989; Maricq & Korenbrot, 1990b). We estimated the model parameters to fit the voltage clamp responses by Maricq and Korenbrot (1988). Since the current depends on both voltage and intracellular calcium concentration, we introduced voltage and calcium dependencies into the activation and inactivation variables (m_{Kc} and m_{Kc1}), respectively, as shown in Table 2.

Intracellular calcium concentration

Several processes affect the intracellular concentration of calcium ions (Yamada *et al.*, 1989). After calcium ions enter the cell through calcium channels, they diffuse into the cell and bind to various buffers such as the protein, calmodulin. Specialized channels act as transporters to extrude calcium ions from the cell. The intracellular mechanisms that control calcium ions in the inner segments are not well understood. We thus modeled the calcium system using the fewest mechanisms necessary to reproduce the calcium dependent currents of the inner segments. Figure 2 shows the schematic illustration of the compartment calcium model. This model is based on the earlier work by DiFrancesco and Noble (1985) in cardiac cells and the recent work on rod outer segments by Torre and his colleagues (1990). Intracellular calcium is controlled by influx via I_{Ca}, by extrusion through the

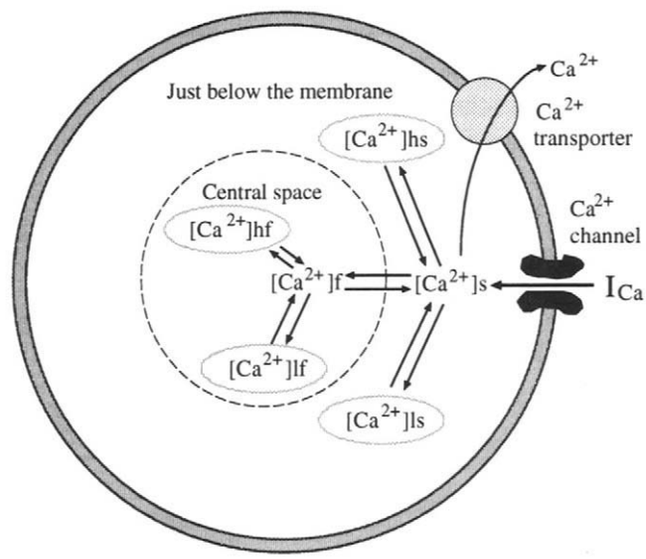

FIGURE 2. Compartment model of intracellular calcium system. The rate of change of internal calcium concentration below the membrane ($[Ca^{2+}]_s$) is determined by influx via I_{Ca}, by extrusion through the transporter, by diffusion into the central space ($[Ca^{2+}]_f$) and by binding and unbinding to high ($[Ca^{2+}]_{hs}$) and low ($[Ca^{2+}]_{ls}$) affinity buffers below the membrane. The calcium ions in the central space ($[Ca^{2+}]_f$) also bind and unbind to the high ($[Ca^{2+}]_{hf}$) and low ($[Ca^{2+}]_{lf}$) affinity internal buffers. See Table 3 for the mathematical formulation.

TABLE 4. Model of phototransduction in retinal rods

Change of intracellular Ca^{2+}

$$\frac{dc}{dt} = b \cdot J - \gamma_{Ca}(c - c_0) - k_1 \cdot (e_T - c_b) \cdot c + k_2 c_b$$

$$\frac{dc_b}{dt} = k_1 \cdot (e_T - c_b) \cdot c - k_2 \cdot c_b$$

$b = 0.625$ [μMsec^{-1} pA^{-1}], $\gamma_{Ca} = 50$ [sec^{-1}],

$k_1 = 0.2$ [sec^{-1} μM], $k_2 = 0.8$ [sec^{-1}], $e_T = 500$ [μM]

Change of intracellular cGMP

$$\frac{dg}{dt} = A - g \cdot (\overline{V} + \sigma \cdot \mathrm{PDE}^*)$$

$$A = \frac{A_{max}}{1 + (c/K_c)^4}$$

$\sigma = 1$ [sec^{-1} μM^{-1}], $A_{max} = 65.6$ [μM sec^{-1}],

$\overline{V} = 0.4$ [sec^{-1}], $K_c = 0.1$ [μM]

Mechanism of phototransduction

$$\frac{dRh}{dt} = J_{hv}(t) - \alpha_1 Rh + \alpha_2 Rh_i$$

$$\frac{dRh_i}{dt} = \alpha_1 Rh - (\alpha_1 + \alpha_3) \cdot Rh_i$$

$$\frac{dT^*}{dt} = \varepsilon Rh \cdot (T_{Tot} - T^*) - \beta_1 T^* + \tau_2 PDE^* - \tau_1 T^* (PDE_{Tot} - PDE^*)$$

$$\frac{dPDE^*}{dt} = \tau_1 T^* \cdot (PDE_{Tot} - PDE^*) - \tau_2 PDE^*$$

$\alpha_1 = 2.0$ [sec^{-1}], $\alpha_2 = 0.8$ [sec^{-1}], $\alpha_3 = 0.6$ [sec^{-1}],

$T_{Tot} = 1000$ [μM], $\tau_1 = 0.2$ [sec^{-1} μM^{-1}], $\tau_2 = 5$ [sec^{-1}],

$\varepsilon = 1.0$ [sec^{-1} μM^{-1}], $PDE_{Tot} = 100$ [μM]

Photosensitive current

$$J = J_{max} \frac{g^3}{g^3 + K^3}$$

$$I_{photo} = Kp \cdot J \cdot (V - Ep)$$

$J_{max} = 5040$ [pA], $K^3 = 1000$ [μM], $Kp = 2$, $Ep = 10$[mV]

Descriptions of phototransduction were summarized from Torre *et al.* (1990).

transporters, and by binding and unbinding to high affinity and low affinity internal buffers. Because our primary aim is to model the action of calcium on the calcium-dependent current, we divided the cell space into two compartments, the space just below the cellular membrane and the central space. The calcium concentration just below the membrane ($[Ca^{2+}]_s$) was used for the calcium-dependent currents. Table 3 shows equations of the present model.

Photocurrent, I_{photo}

The biophysical processes underlying phototransduction are now well understood (Yau & Baylor, 1989; McNaughton, 1990), and a quantitative model of phototransduction has been proposed by Torre *et al.* (1990). In order to simulate the light response of photoreceptors, we introduced the flow of photocurrent into the inner segment as shown in Fig. 1. In the model of phototransduction, the cyclic GMP-activated current (J) is expressed as a function of the concentration of cyclic GMP (g). The cyclic GMP-activated current can be measured in an excised patch condition, and it is sufficient to use the current, J, for reproducing the current response in the outer segment. The current–voltage relation of the cyclic GMP-activated current shows an outward rectification reversing near at +10 mV, and thus the photocurrent flow into the inner segment depends on the membrane potential (Baylor & Nunn, 1986). We expressed the voltage dependency of photocurrent (I_{photo}) by multiplying the cyclic GMP-activated current (J) by the electrochemical driving force ($V - E_p$) as shown in Table 4.

SIMULATED RESPONSES OF THE PHOTORECEPTOR MODEL

Voltage-clamp simulation

Under voltage-clamp conditions, total membrane current (I) in the inner segment is described as:

$$I = I_{Ca} + I_{Kv} + I_h + I_{Cl(Ca)} + I_{K(Ca)} + I_l. \quad (3)$$

Voltage-clamp simulations were made under the conditions identical to electrophysiological experiments by Maricq and Korenbrot (1988). Figure 3(A) shows the simulated total ionic current under three different pharmacological conditions corresponding to control, TEA-contained, and TEA- and Co^{2+}-contained solutions. In these conditions, external solutions always contain Cs^+, and thus we blocked I_h completely. The current responses with TEA are simulated by reducing $\overline{g_{Kv}}$ from 2.0 nS to 0.16 nS, because the current dynamics under the TEA–Co solution still shows a slight delayed-rectifier component [Fig. 2 of Maricq & Korenbrot (1988)]. Figure 3(B) shows the current–voltage relation measured from the TEA responses. The currents were measured at the peak, 5 msec after the onset of the depolarizing pulse and 135 msec after the onset of the command pulse. The experimental observations are well reproduced by our model.

Each ionic current simulated under control conditions is shown in Fig. 3(C). From these responses we can explain how the complicated current responses in Fig. 3(A) are generated. An early inward current elicited by the voltage step to -20 mV is I_{Ca}, and the following outward component is mostly $I_{Cl(Ca)}$ due to the increase of the calcium concentration ($[Ca^{2+}]_s$). The voltage step to 0 and +20 mV activates the outward currents, I_{Kv} and $I_{Cl(Ca)}$. The voltage step to +40 mV activates I_{Ca} to a lesser extent than the voltage step to 0 or +20 mV, thus the calcium concentration increases slowly and is reduced compared to these voltage clamp levels. As a result, $I_{Cl(Ca)}$ is smaller and slower compared to the current elicited by 0 and +20 mV voltage steps.

Current clamp simulation

The ionic current models are derived by the data from voltage-clamp experiments, and thus there are no interactions among ionic currents. Here we simulate current clamp responses to validate the proposed model using an independent set of data. The current clamp simulation is a critical test of the ionic current model, since there is no guarantee that the model can reproduce the current clamp responses, in which the simulation has to be made by using the whole components [see discussion in Usui *et al.* (1996c)]. Maricq and Korenbrot (1988) showed that, in isolated lizard cones, action potentials can be generated by depolarizing current steps. The corresponding spike responses simulated by our model are shown in Fig. 4.

The responses elicited by the depolarizing current under control and TEA conditions are reproduced well. Dotted traces in Fig. 4(A and B) are results simulated by blocking $I_{Cl(Ca)}$ in the model. Current dynamics during spike responses are shown in Fig. 4(C and D). From these results, we can understand which ionic current participates in the different phases of the spike responses. The

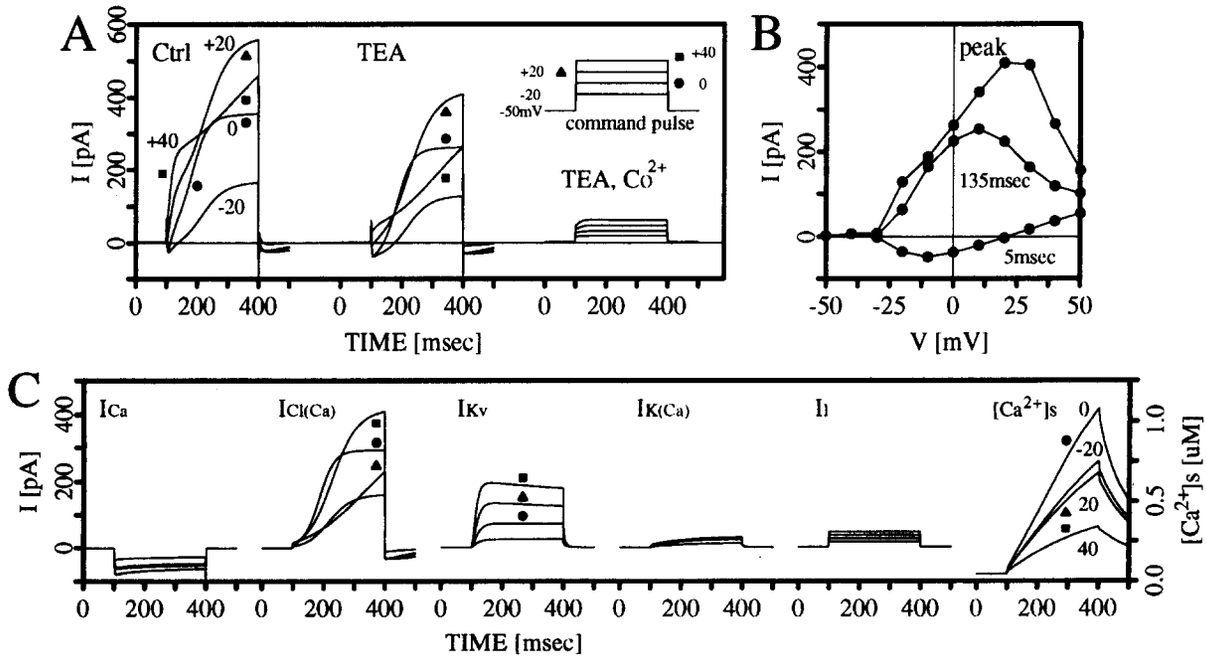

FIGURE 3. Simulated responses of the inner segment model under voltage clamp conditions. (A) Membrane currents under three different conditions corresponding to control, TEA and TEA–Co solutions. The TEA responses were simulated by reducing $\overline{g_{Kv}}$ from 2.0 to 0.16 nS. (B) Current–voltage relation at the peak, 5 msec, 135 msec, measured from the TEA responses. (C) Ionic current components and calcium concentration under control condition.

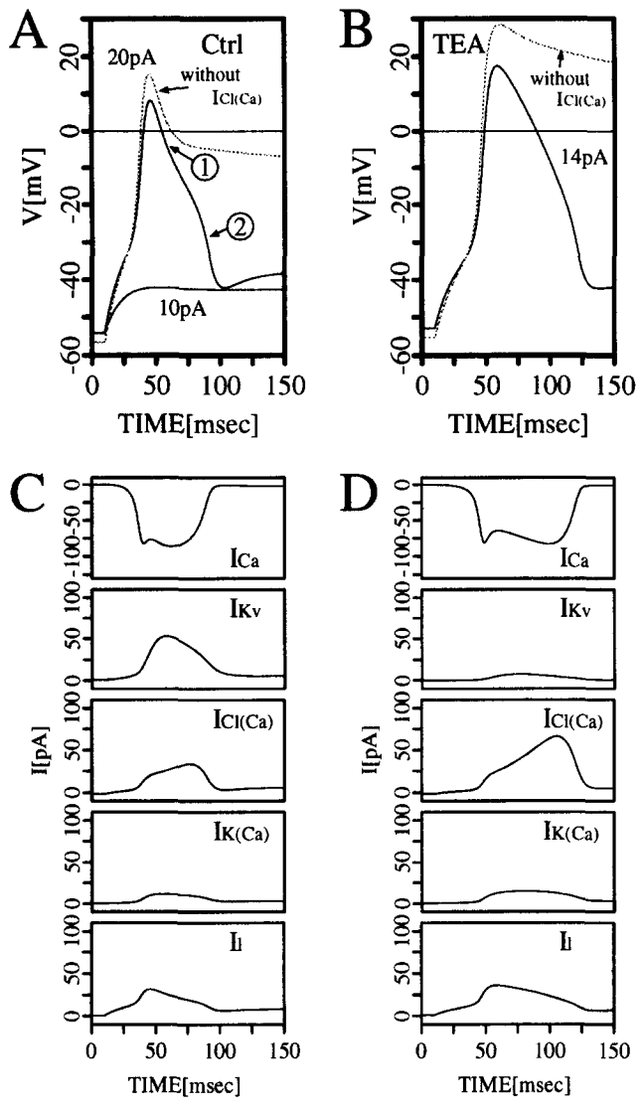

FIGURE 4. Simulations of the current-clamp experiments using the inner segment model. (A) Voltage responses of the model to depolarizing current steps of 10 and 20 pA under control condition. The response without $I_{Cl(Ca)}$ is plotted by the dotted line. (B) Voltage response of the model to a depolarizing current step of 14 pA under the TEA condition. $\overline{g_{Kv}}$ = 0.16ns for the TEA condition. Dotted trace was simulated by blocking $I_{Cl(Ca)}$. (C and D) Ionic current components under the control and TEA conditions, respectively.

membrane depolarization initially elicited by the applied current activates I_{Ca}, and I_{Ca} further depolarizes the cell. I_{Kv} and $I_{Cl(Ca)}$ participate in repolarization of the action potential in phases 1 and 2, respectively. As clearly shown by the dotted traces in Fig. 4(A and B), the membrane potentials remain depolarized without $I_{Cl(Ca)}$, that is, $I_{Cl(Ca)}$ terminates the action potential.

Simulated light responses of the rod photoreceptor

In general, ionic current models are typically used in the context of voltage- and current-clamp experiments. They can also be used in studies investigating several sorts of dynamical behaviors. Here we simulate light responses of rod photoreceptors.

Figure 5 shows the responses of photocurrent (A) and photovoltage (B) to a series of light flashes of increasing intensity. The model produces responses highly similar to those measured experimentally (Baylor *et al.*, 1984). In order to assess the importance of each ionic current in shaping the voltage response to light, we estimated the ionic current flow during the light responses as shown in Fig. 5(C). From these responses, we can explain why the voltage response of a rod to a bright flash is not the mirror image of the photocurrent. In normal conditions, I_h activates slowly as the membrane hyperpolarizes, and thus I_h shapes the initial transient in the voltage response. To confirm the effects of I_h, we simulated the responses by blocking I_h in the model as shown in Fig. 5(D). The voltage responses changes dramatically. The initial transient for bright stimuli disappeared, the time to peak of the voltage response was delayed, the amplitude was increased, and the duration of the response was prolonged. These results are consistent with the experimental result by Baylor *et al.* (1984), who showed that

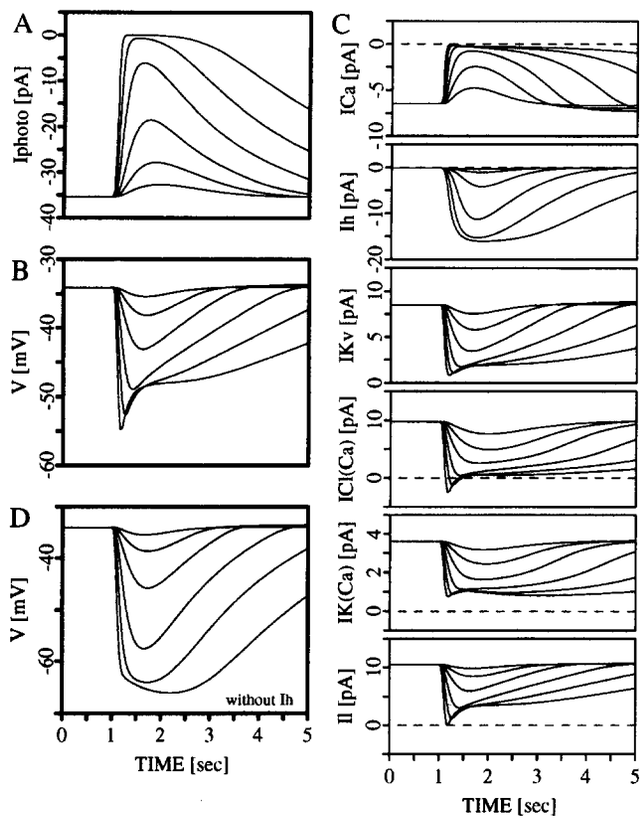

FIGURE 5. Simulated light responses of the photoreceptor. Stimulus intensities [$J_{hv}(t)$] were 0.03, 0.1, 0.3, 1.0, 3.0, 10.0 $Rh^*_t\ sec^{-1}$. The duration was 50 msec. (A) Photocurrents; (B) voltage responses; (C) each ionic current of the inner segment; (D) voltage responses without I_h. $Cl_h = 0.45\ \mu M$, $A_{max} = 131.2\ \mu M\ sec^{-1}$, $\bar{V} = 0.8\ sec^{-1}$, $\overline{g_h} = 3.0$ nS, $\alpha_h = \frac{8}{\exp((V+78)/14)+1}$, $\beta_h = \frac{18}{\exp(-(V+8)/19)+1}$ for simulating the rod responses.

the initial spike characteristics of rod responses was abolished by the I_h blocker, Cs.

Simulated oscillatory photoresponses of rods

Several experimental studies have shown that the membrane potential of rods oscillate under certain conditions (Normann & Pochobradský, 1976; Fain *et al.*, 1980; Yamada & Tauchi, 1982). These previous results suggest that the oscillations result from interactions with other retinal neurons (Normann & Pochobradský, 1976), or originate in rods themselves (Fain *et al.*, 1980; Yamada & Tauchi, 1982).

Figure 6 shows the oscillatory responses simulated by our model. The oscillations were observed after the potential returns to the resting level after the bright stimulus. These observations are quite similar to that of Normann and Pochobradský (1976). The simulations, however, were made by a single photoreceptor model, and thus the result strongly suggests that the oscillations are initiated in rods.

Figure 7 shows I_{Ca}, $I_{Cl(Ca)}$ and calcium concentrations ($[Ca^{2+}]_s$, $[Ca^{2+}]_{ls}$) during the oscillatory response. These behaviors can be explained by the calcium-dependent interactions. During the repolarizing phase of the light response, $[Ca^{2+}]_s$ and $[Ca^{2+}]_{ls}$ are reduced, which cause a decrease of $I_{Cl(Ca)}$ and result in membrane depolarization [A in Fig. 7(B)]. The depolarization activates I_{Ca}, which in turn increases $[Ca^{2+}]_s$. An increase of $[Ca^{2+}]_s$ activates calcium-dependent outward currents ($I_{Cl(Ca)}$, $I_{K(Ca)}$), which causes membrane hyperpolarization [B in Fig. 7(B)]. This process continues until $[Ca^{2+}]_{ls}$ reaches the steady-state. These calcium interactions are further enhanced by blocking I_{Kv} and increasing the extracellular calcium concentration as shown in Fig. 8. The simulated responses agreed well with the experimental recordings by Fain *et al.* (1980).

DISCUSSION

In this paper, an ionic current model of the vertebrate photoreceptor was proposed. We have obtained a satisfactory agreement between simulated and experimental responses. The model reproduced the voltage- and current-clamp responses reasonably well and the light response properties observed in rod photoreceptors.

Attwell and Wilson (1980) modeled the time- and voltage-dependent current in rods, and analyzed the electrical behavior of rods using model simulations. They found that the current, I_A, plays a major role in shaping the light responses. Since their I_A is an inward current activated by membrane hyperpolarization, the current partially corresponds to I_h in our model. They did not separate membrane current into each ionic current, because the components were not fully identified in

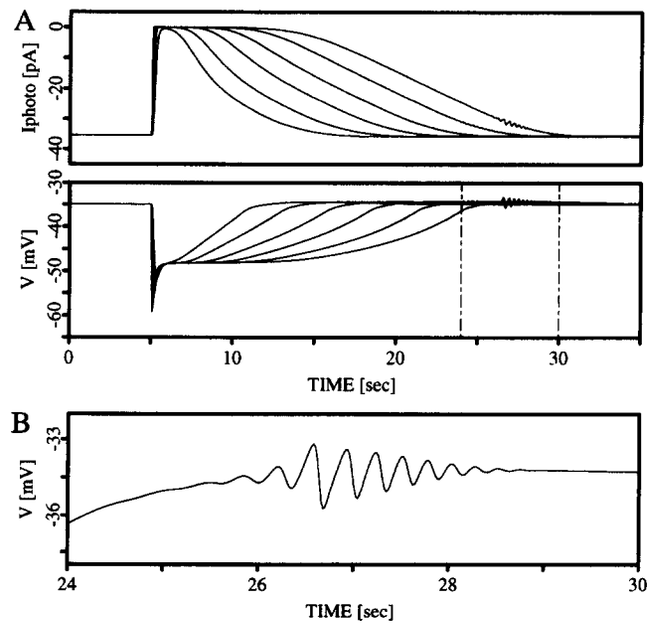

FIGURE 6. Simulated oscillatory photoresponses of rod. (A) Simulated responses of photocurrent and photovoltage. The intensity of $J_{hv}(t)$ was 1.0, 3.0, 10.0, 30.0, 100.0, 300.0 $Rh_t^*\ sec^{-1}$. The oscillations were observed after the potential returns to the resting level in response to a stimulus of intensity, $J_{hv}(t)$ of 300 $Rh_t^*\ sec^{-1}$. $\overline{g_{Ca}} = 1.5$ nS, $\overline{g_{Kc}} = 1.0$ nS, $\overline{g_{Kv}} = 2.4$ nS, $Cl_h = 0.45\ \mu M\ sec^{-1}$, $E_{Cl} = -55$ mV for fitting the voltage response to that of Normann and Pochobradsky (1976). (B) The oscillatory response on an expanded time scale for the maximum intensity.

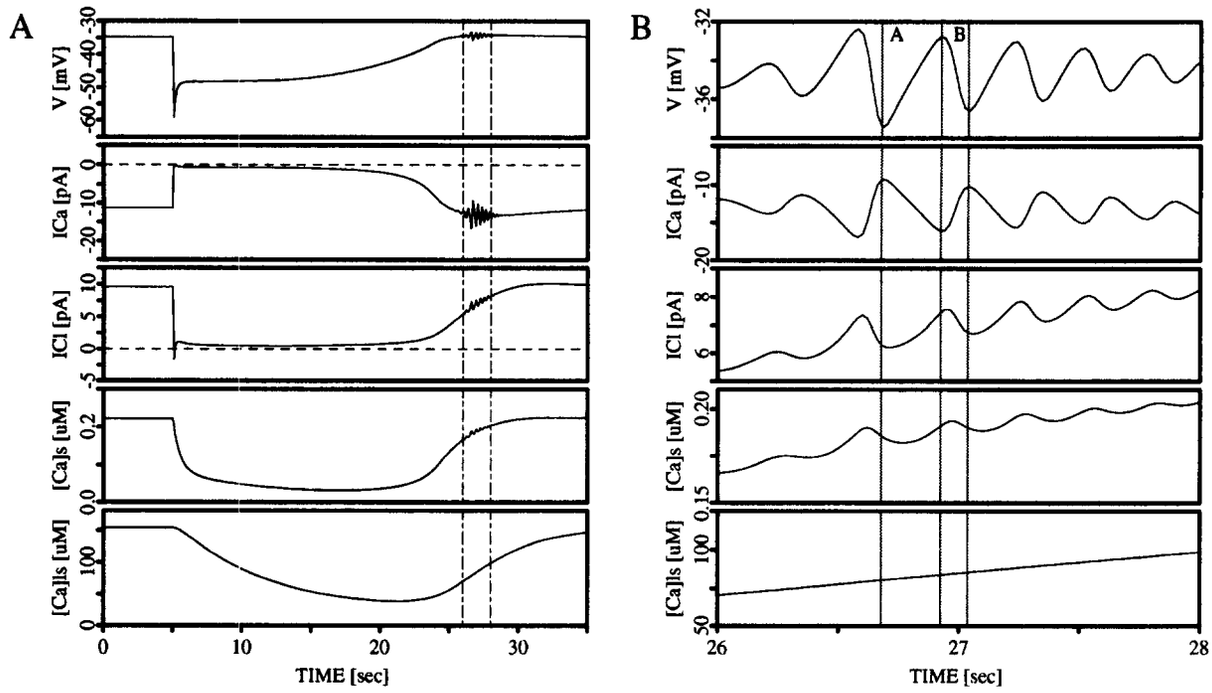

FIGURE 7. The time course of ionic current and intracellular calcium concentrations during the oscillatory response. (A) Calcium-dependent components of the model during the oscillation. (B) The same as (A) except in the expanded time scale. See text for further explanation.

1980. Our model, however, takes into account many of the ionic current components. This level of details in the model makes it possible to predict the responses under various conditions. The predicted effects of I_h on the light responses suggest that I_h makes the response more transient as the membrane potential hyperpolarizes, which is consistent with the experimental finding by Baylor *et al.* (1984). We also found that zatebradine, a drug with a specific bradycardiac action, might induce visual symptoms as a side effect by blocking I_h channels in rods (Usui *et al.*, 1996b).

Oscillatory responses in rods have been an interesting issue of retinal physiology, since the responses provide a key to understand the ionic mechanisms in rods and/or synaptic interactions between rods and other neurons. We demonstrated that the model of a single rod shows oscillatory responses under the conditions corresponding to the physiological experiments. The result implies that negative feedback loops among components of the

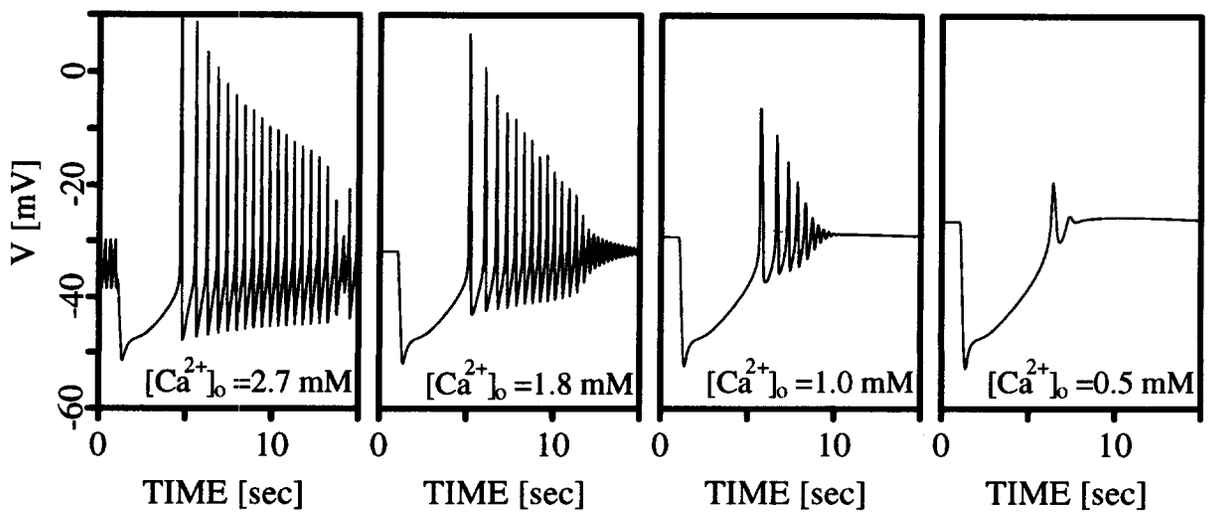

FIGURE 8. Simulated spike responses in rods by the model. The responses correspond to experimental recordings by Fain *et al.* (1980). The spike responses strongly depend on the extracellular calcium concentration. $\overline{g_{Ca}}$=1.5, 0.9, 0.5, 0.3 nS for representing the conductance change by the extracellular calcium concentration. $\overline{g_{Kv}}$ for the TEA condition.

calcium system might generate the oscillations in rods. A detailed analysis of the intracellular calcium system is needed to verify the proposed mechanism for oscillatory behavior.

The present model is able to account for many features of experimental observations in photoreceptors but not all the findings. Ionic currents identified in synaptic terminal (Kaneko & Tachibana, 1986) of cone photoreceptors were not involved in the present model. The detailed mechanism of phototransduction in cones are not also well understood yet. We still have to work out to develop a quantitative model of phototransduction in cones to simulate the light responses.

REFERENCES

Attwell, D. & Wilson, M. (1980). Behaviour of the rod network in the tiger salamander retina mediated by membrane properties of individual rods. *Journal of Physiology, 309*, 287–315.

Bader, C. R., Bertrand, D. & Schwartz, E. A. (1982). Voltage-activated and calcium-activated currents studied in solitary rod inner segments from the salamander retina. *Journal of Physiology, 331*, 253–284.

Barnes, S. & Hille, B. (1989). Ionic channels of the inner segment of tiger salamander cone photoreceptors. *Journal of General Physiology, 94*, 719–743.

Baylor, D. A., Matthews, G. & Nunn, B. J. (1984). Location and function of voltage-sensitive conductances in retinal rods of the salamander, ambystoma tigrinum. *Journal of Physiology, 354*, 203–223.

Baylor, D. A. & Nunn, B. J. (1986). Electrical properties of the light-sensitive conductance of rods of the salamander *Ambystoma tigrinum*. *Journal of Physiology, 371*, 115–145.

DiFrancesco, D. & Noble, D. (1985). A model of cardiac electrical activity incorporating ionic pumps and concentration changes. *Philosophical Transactions of The Royal Society, 307*, 353–398.

Fain, G. L., Gerschenfeld, H. M. & Quandt, F. N. (1980). Calcium spikes in toad rods. *Journal of Physiology, 303*, 495–513.

Hodgkin, A. L. & Huxley, A. F. (1952). A quantitative description of membrane current and its application to conduction and excitation in nerve. *Journal of Physiology, 117*, 500–544.

Kaneko, A. & Tachibana, M. (1986). Effects of γ-aminobutyric acid on isolated cone photoreceptors of the turtle retina. *Journal of Physiology, 373*, 443–461.

Maricq, A. V. & Korenbrot, J. I. (1988). Calcium and calcium-dependent chloride currents generate action potentials in solitary cone photoreceptors. *Neuron, 1*, 503–515.

Maricq, A. V. & Korenbrot, J. I. (1990a) Inward rectification in the inner segment of single retinal cone photoreceptors. *Journal of Neurophysiology, 64*, 1917–1928.

Maricq, A. V. & Korenbrot, J. I. (1990b) Potassium currents in the inner segment of single retinal cone photoreceptors. *Journal of Neurophysiology, 64*, 1929–1940.

McNaughton, P. A. (1990). The light response of vertebrate photoreceptors. *Physiological Reviews, 70*, 847–883.

Normann, R. A. & Pochobradský, J. (1976). Oscillations in rod and horizontal cell membrane potential: Evidence for feed-back to rod in the vertebrate retina. *Journal of Physiology, 261*, 15–29.

Torre, V., Forti, S., Menini, A. & Campani, M. (1990). Model of phototransduction in retinal rods. *Cold Spring Harbor Symposia on Quantitative Biology, 55*, 563–573.

Usui, S., Ishihara, A., Kamiyama, Y. & Ishii, H. (1996c). Ionic current model of bipolar cells in the lower vertebrate retina. *Vision Research, 36*, 4069–4016.

Usui, S., Kamiyama, Y., Ishii, H. & Ikeno, H. (1996a). Reconstruction of retinal horizontal cell responses by the ionic current model. *Vision Research, 36*, 1711–1719.

Usui, S., Kamiyama, Y., Ogura, T., Kodama, I. & Toyama, J. (1996b). Effects of zatebradine (UL-FS 49) on the vertebrate retina. In Toyama, J., Hiraoka, M. & Kodama, I. (Eds), *Recent progress in electropharmacology of the heart* (pp. 37–46). Boca Raton: CRC Press.

Wollmuth, L. P. & Hille, B. (1992). Ionic selectivity of I_h channels of rod photoreceptors in tiger salamanders. *Journal of General Physiology, 100*, 749.

Yamada, W. M., Koch, C. & Adams, P. R. (1989). Multiple channels and calcium dynamics. In Koch, C. & Segev, I. (Eds), *Methods in neuronal modeling* (Chap. 4, pp. 97–133). Cambridge MA: The MIT Press.

Yamada, M. & Tauchi, M. (1982). Oscillatory photoresponses of rods in the light-adapted bullfrog retina. *Biomedical Research, 3*, 143–147.

Yau, K. W. & Baylor, D. A. (1989). Cyclic GMP-activated conductance of retinal photoreceptor cells. *Annual Reviews in Neuroscience, 12*, 289–327.

Acknowledgements—This work was supported in part by the Human Frontier Science Program (HFSP; P.I.: H. Spekreijse), and the Grant-in-Aid for Scientific Research on Priority Areas (No. 05267104), the Ministry of Education, Science, Sports and Culture of Japan.